Moringa oleifera seeds extracts / Magnetite based bionanocomposites for hexavalent chromium uptake

Tafadzwa Shekede [1], Ajay Kumar Mishra

[1]*Nanotechnology and Water Sustainability Research Unit, College of Science, Engineering and Technology, University of South Africa, Florida Campus, Johannesburg, South Africa.*

[2] *Department of Mine Survey, University of Johannesburg, Doornfontien Campus, Corner Siemert & Louise Street, P Box 17011, Doornfontein ,2028 Johannesburg, South Africa.*

[3]*Institute for the Development of Energy for Africa Sustainability, College of Science, Engineering and Technology, University of South Africa, Florida Campus, Johannesburg, South Africa.*

[#]*Corresponding author: tshekede@uj.ac.za*

ABSTRACT

Sequestration of hexavalent chromium six Cr (VI) from wastewater is a big challenge due to its high toxicity and threat to living organisms. In this investigation, highly ordered mesoporous magnetite nano particles functionalised with protein extracts from de-oiled Moringa seeds were synthesised. High-resolution TEM (HRTEM) and Scanning electron microscopy (SEM/EDS) results showed good dispersion of organic compounds on de-oiled Moringa oleifera iron nano particles in water (DMOSFeNP $_{H2O)}$ compared to the other two bionanocomposites i.e. DMOSFeNPsalt and DMOS biocomposite ($DMOS_{biocomp}$) The DMOSFeNP $_{H2O}$ exhibited good separability in effective removal of Cr (VI). The capping of the magnetite with Moringa water extracts greatly improved the removal efficiency of Cr (VI) to 80 % at equilibrium time. The adsorption of Cr (VI) ions by $DMOSFeNP_{H20}$, DMOSFeNPsalt and $DMOS_{biocomp}$ followed Fraundlich and Langmuir adsorption isotherm model with R^2 values of 0.94, 0.77 and 0.67 respectively. The Pearson's correlation coefficient showed that the adsorption process was 1^{st} order kinetics for DMOSFeNP $_{H2O}$ and 2^{nd} order for DMOSFeNP $_{salt}$ and $DMSO_{biocomp}$

indicating chemisorption and physio sorption reactions. In this investigation, the functionalisation was done using crude salt and water extracts from Moringa Oleifera seeds, and this of its kind in adsorption of Cr (VI) in aqueous solution.

Keywords: Cr (VI); Magnetite; Bionanocomposite; Moringa oleifera; Adsorption isotherms; Kinetic models.

1.0 Introduction

Of the total water on earth, only 0,0008% is available and renewable in rivers and lakes in addition to the water that falls as rain or snow or that has been accumulated and stored as groundwater. It is estimated that by the year 2025, there will be 4-5 billion people on earth who will live in regions already lacking sufficient clean water [1]. Heavy metals are elements with atomic density greater than 6g/cm^3, such as chromium (Cr^{6+}) , copper (Cu^{2+}) cadmium ,(Cd^{2+}), lead (Pb^{2+}) and zinc (Zn^{2+}) and are the most persistent pollutants in waste water as a result of overpopulation and expansion of industrial activities [2].

Hexavalent chromium has been recognised as one of the major toxic substances by United States Environmental Protection Agency (USEPA), because of its carcinogenic effects and recommended limits in drinking water is 0,05-1mg/L. [3]. Most of the Cr (VI) pollution comes from the tanning industries. Chromium generally exists as non-toxic and immobile trivalent (Cr (III) and hexavalent (Cr (VI) which is readily soluble in water. [4]. Generally, Cr containing effluents contaminate the environment at their point of disposal where Cr (III) undergoes oxidation and forms Cr (VI). In acidic medium, hexavalent chromium exists as a tetraoxohydrochromate ($HCrO_4^-$) and dichromate ($Cr_2O_7^{2-}$) species and at alkaline pH, it is present as a tetraoxochromte (CrO_4^{2-}) in solution. Hexavalent chromium is more mobile while

the trivalent form is less toxic and strongly retained in the soil. However, it is probable for the trivalent chromium to be oxidized to the hexavalent state due to the manganese oxides in the soil. [5]; [6]; [7]; [8]; [9]; [10]; [11].

Removal of Cr (VI) is achieved by various physico-chemical processes such as oxidation/reduction, precipitation /filtration, coagulation, ion exchange and membrane separation. High costs and process complexity have limited their use in industries. Varieties of technologies involving chemical reduction, electrochemical and biological methods are reported for the remediation of the hexavalent chromium. [12]; [13]. Among these, changing the oxidation state of the hexavalent chromium by chemical reduction using reducing agents such as bisulphate followed by precipitation of the trivalent chromium as hydroxide using lime or alkali is extensively used in the effluent treatment. The precipitated chromium is usually recovered by dissolution in sulphuric acid [14]. However, during the precipitation of the trivalent chromium from the ternary wastewater, a considerable amount of sludge is generated, and this increases the overall cost of the treatment process. The adsorption on the oxide surfaces such as pure peroxide, modified titanium dioxide and goethite is very useful in the removal of Cr (VI) [15]. Reduction to the trivalent state coupled with adsorption on a suitable matrix is also a viable option [16]. Photo catalytic reduction by titanium (TiO_2) coupled to functionalised carbon nanotubes is very effective in the conversion of the hexavalent chromium to trivalent state [17]. Humic acid coated magnetite and magnetic nano particles are also very effective to reduce +6 to +3 state, which is less toxic. [18].

For in-situ remediation, iron has good ability to reduce the hexavalent chromium. The trivalent Cr (III) is absorbed on the iron hydroxides as inner sphere complexes [19]. Polycrystalline haematite is one of the recently reported materials for the reduction of chromate (VI) [20]. An

adsorption capacity of 1.67mmol/g was achieved using polyaniline nanowires, which involved adsorption as well as reduction of chromium to the +3 oxidation state. This adsorbent shows good potential in the treatment of the wastewater [21]. Low cost adsorbents involving various forms of activated carbons are some of the classical materials that are tested for the remediation of the chromium with good performance efficiency [22, 23]. Adsorption coupled with reduction of hexavalent chromium was thoroughly investigated using agricultural waste [24]. Carbonaceous adsorbents prepared from sunflower stem has an adsorption capacity of 53.7mg/g for Cr (VI) [25]. In addition to activated carbon, several other low waste materials such as zeolites, chitosan and waste slurry are other useful adsorbents for the removal of hexavalent chromium [26]. Cationic inorganic materials are also effective in sequestering anionic pollutants. In this regard, zeolites modified with quaternary ammonium surfactants remove chromate from aqueous medium through electrostatic interaction mechanisms [27]. Nitrogen enriched activated carbon using bamboo residue yields 89% adsorption efficiency at 100mg/l Cr (VI) concentration [28]. A magnetic lignin composite adsorbent with an adsorption capacity of 123mg/g and a regeneration efficiency of 87% for five cycles using sodium hydroxide was very effective in the adsorption of Cr (VI) [29]. A higher adsorption capacity of 250mg/g at pH 5 was achieved using magnetite porous fibres prepared by a protein assisted hydrothermal process. The adsorbed chromium was also easily desorbed using dilute nitric acid solution. With 100mg/l Cr (VI), the removal efficiency was retained up to 80% after four cycles [30]. A novel metal organic hybrid copper(I) metallo-gel adsorbent was also studied for the reductive removal of Cr(VI) to Cr(III) followed by adsorption with a high adsorption capacity of 331mg/g at p H 2.7 [31].

In recent years, use of low costs adsorbents have been considered to reduce the Cr concentration in tannery effluents. Adsorption could be a good alternative technology for the removal of

heavy metals, especially at low concentration. The efficiency of adsorption depends on the adsorbent surface area, surface morphology, pore size distribution, polarity and functional groups attached to the adsorbent surface [32]. The principle types of adsorbents include activated carbon, synthetic polymers and silica based adsorbents, however these adsorbents are seldom used for wastewater adsorption because of their high cost [33].

Agricultural waste is abundant and hence many studies utilise agricultural by-products as adsorbents. Using agricultural waste serves double purpose i.e. it converts unwanted, surplus agricultural waste to useful value-added adsorbents and saves high preparation costs of the prepared adsorbents [34]. The adsorbents may be of organic or biological origin, modified materials, nano sized materials, industrial by-products or mineral substance, modified bio-polymers, biomass bio-adsorbents, modified agricultural waste and biological waste [35]. Some of the cleaner technology methods developed up to date using agricultural waste are very expensive to use and give rise to new waste streams which need further processing as a sustainable measure to reduce environmental impacts [36].

Nano crystalline and metal oxides have attracted international interest from researchers over the years due to their unusual physical and surface chemical and catalytic properties, cost effective, biodegradability and environmentally friendly nature. Among the metal oxide nanoparticles, iron oxide magnetic nanoparticles are of great interest to many scientists in recent years because of their small size, good stability, low cost, high magnetic permeability and large surface for unique physio-chemical properties. Isolated nanoparticles exhibit amazing properties and when mixed with other materials, the resultant compound attains improved properties because of the increased surface to volume ratio. Fe ions may be used to catalyze Fenton-like reactions for the generation of hydroxyl radicals using strong oxidizing

agents as precursors. Hydroxyl radicals have high oxidation potential and can degrade organic molecules such as dyes generated in textile effluents [37]. There are many plant based bionanocomposite materials available on the market.

The aim of this study was to evaluate the effectiveness of using de-oiled Moringa oleifera seeds extracts modified bionanocomposites to remove Cr (VI) ions from waste solution. Understanding of the interaction between the modified magnetite bionanocomposite of Moringa oleifera seed and the contaminated water is fundamental to the adsorption mechanisms and regeneration of the absorbent. The overall goal was to increase surface area of adsorption and capitalize on the magnetic properties of the bionanocomposites for ease regeneration of the biosorbent. In this study, the functionalization was done using crude salt and water extracts from de-oiled Moringa oleifera seeds, and this is first of its kind in removal of Cr (VI) ions in aqueous solution. The work is relatively novel because the synthesis route does not require hazardous chemical and yields an ecogreen benign magnetite nanoparticles.

Material and methods

2.1 Materials

Moringa oleifera seeds was obtained from Limpopo province, Republic of South-Africa. Stock standards for Cr (VI) were prepared by diluting pure standard solutions of the potassium dichromate ($K_2Cr_2O_7$) in distilled water. The 1000-ppm standard solution of $K_2Cr_2O_7$ were sourced from Associated Chemical Enterprises (Pvt), South Africa. Hydrated iron chloride ($FeCl_2$/$FeCl_3$) were purchased from Merck, Darmstadt Germany. All other reagents were of analytical grade and used without further treatment. Deionised water was prepared by a Milli-Q system.

2.2 Sample preparation:

2.2.1 Preparation of de-oiled Moringa oleifera seeds:

Moringa oleifera seeds were cleaned in water and dried in an oven for 2 hours before being crushed and sieved through a 350µm sieve. The crushed seeds were heated for 24 hrs in a Soxhlet apparatus using normal hexane to remove the oil before drying at 50 ^{o}C to a constant dry weight in an oven. A 26,75 extractive removal percentage oil by wt/wt using normal hexane was used for the preparation of the low-cost magnetite bio-composite material for the experiments.

2.2.2 Preparation of the de-oiled Moringa oleifera seed bio-composite:

The de-oiled Moringa oleifera coated magnetite bio-composite was synthesised by co-precipitation technique. Fifty grams de-oiled Moringa oleifera seeds were mixed with 1M$FeCl_2$ and 0.5M$FeCl_3$ as precursors in a 500ml beaker. The mixture was immersed in a water bath with continuous steering at a temperature of 80^{o}C for a period of 2 hrs in an alkaline media i.e. pH 10. The solution underwent dehydration followed by decomposition with evolution of gases resulting in a colour change from dark brown to reddish brown paste. The paste was collected and transferred into a centrifugal machine at 2000 rpm for 5mins to dehydrate the sample. The sample was transferred to an oven and dried at 80^{o}C for 24hrs. The dried sample was crushed to powder and sieved through a 350µm sieve for the adsorption experiments.

2.2.3 Synthesis of Moringa oleifera modified magnetite iron oxide nanoparticles through co-precipitation method:

Before preparation of Moringa oleifera seed extracts, the seeds where de-oiled in a Soxhlet apparatus for 24 hrs with normal hexane and dried in an oven for 12 hrs at 60° C. They were

then crushed to 350µm sieve size. 1.25g defatted seeds were mixed with 7.305g of NaCl in a 250ml volumetric flask and filled with de-ionized water to obtain the salt extract. After stirring for 2hrs at 200rpm in an orbital shaker, the solution was filtered using Whatman 42 filter paper. The water extract was prepared by mixing 1.25g of de-oiled Moringa seeds with 250ml de-ionised water. The process follows the same procedure for the preparation of the salt extract. The magnetite iron oxide nano particles were synthesised via co-precipitation methods using the crude extracts solutions from de-oiled Moringa oleifera seeds. Synthetic procedure was done according to procedure by Wang et al. (2011), with some few modifications. The iron source was prepared by dissolving 5.88 g of $(NH_4)_2Fe\ (SO_4)_2.6H_2O$ and 8.10 g of $FeCl_3.6H_2O$ in 100ml deionized water. The resultant solution was mixed in an orbital shaker at 200rpm for 10mins. The $Fe^{2+/}Fe^{3+}$ mixture was transferred to an autoclave reactor and mixed with 3ml of the prepared salt extract solution. The contents of the reactor were heated slowly to 80^{o}C in an inert atmosphere of nitrogen gas with continuous steering at 1200rpm. Dropwise addition of the prepared 10% ammonia solution was done when the contents of the reactor reached 80^{o}C.The reaction was allowed to proceed for 2 hours at 80^{o}C under a nitrogen atmosphere with a pressure and gas flow rate of 2000Kpsi and 0.4L/sec respectively. After 2 hrs, the reactor was cooled, and the resultant supernatant solution was separated from magnetite using a centrifuge at 3000rpm for 1 hour. The magnetite nanoparticles were washed several times in distilled before vacuum dried at 50^{o}C for 12hrs. After drying the magnetite nanoparticles were crushed to 350µm sieve size and stored in desiccator.

2.3 Characterisation of the magnetic bio composites.

An atomic absorption spectrometer (AAS) (ICE 300 Series) was used to determine the chemical elements using adsorption of optical radiation by free atoms in gaseous state. Fourier

infrared spectrum analysis (FTIR) of magnetite bionanocomposites were done over the range of 4000-400cm^{-1} to determine the functional groups in the bionanocomposite. The measurements were carried out on a Nicolet ISO10 Series FTIR Spectrometer. To determine the crystallinity phases of the functionalised Moringa oleifera bionanocomposites formed, X-ray diffraction (XRD) analysis were done by a Rigaku ZXS Primus (II) instrument (Rikagu, Japan) with Cu-Kα radiation source with wave length of 0.154nm and was operated at 40Kv/30Ma over2θ range of 2-800. The scanning speed was maintained at 50 min^{-1}. The morphology of the optimised Moringa oleifera bionanocomposites was analysed using High-resolution transmission electron microscopy (HR-TEM, JEOL JEM-200, Japan). The nanoparticles were stained with uranyl acetate solution before observation. Ultrasonification of the samples were done at 42^{o}C for 10mins. Samples were allowed to dry before they were mounted on copper grids for HRTEM analysis. Surface morphology and shape of the Moringa oleifera bionanocomposites were characterised by scanning electron microscopy coupled with energy dispersive X-ray spectroscopy (SEMEDS) (Vega 3 xmu with Oxford X-max EDS system) after carbon coating the samples in Quorum Q150E. A Micrometrics Accelerated Surface Area Porosimetry (ASAP) 2000 nitrogen adsorption apparatus was used to characterise the Brunauer-Emmet-Teller (BET) surface area of the Moringa oleifera bionanocomposites. Physical properties of the bionanocomposites were determined with a nitrogen absorber, System 2020(ASAP) Micrometrics at (197.382Oc). Prior to nitrogen adsorption measurements, the sample was degassed under vacuum at 250^{o} C for 12 hours.

2.4 Swelling studies experiments for DMOS.

2.4.1 Swelling experiments:

Swelling experiments were performed by weighing between 1.5 g of the de-oiled Moringa oleifera seeds with size ranges between 710µm - 18mm. Weighed samples were mixed with a fixed volume of water and transferred to an orbital shaker at 140rpm for 150mins. Samples were collected at 30 mins intervals to determine maximum swelling percentage for each sieve size. The percentage swelling was calculated using the following equation 1:

$$\%M_t = \frac{(C_i - C_f)}{C_i} \quad (1)$$

Where C_i is the initial mass of the Moringa oleifera seed before swelling and C_f is the final mass of Moringa oleifera seed after water swelling time t. Swelling curves were obtained by plot of Mt vs time (t).

2.4.2 Batch adsorption experiments on the synthesised DMOS bio composite ($DMOS_{biocomp}$):

All the batch adsorption experiments were performed by the ultrasound assisted method.10-25mls aliquots of the aqueous solutions containing approximately 95ppm of Cr (VI) ions with adsorbent dosage range of 0,002-0, 05 mg/25ml at pH ranges of 4-6 and ultra sound time of 30mins. The resultant solution was filtered and analysed by an AAS. The metal removal efficiency was calculated using the following equation:

$$\%R = \frac{(C_0 - C_t)}{C_0} \quad (2)$$

where C_0 (mg/L) and C_t (mg/L) are the concentrations of the Cr (VI) ions at the initial and after time t, respectively. The adsorbed amount of the metal ions (q_e (mg/g) was calculated using the following mass balance equation:

$$q_e = \frac{(C_0 - C_e)V}{W} \quad (3)$$

Where C_0 and C_e (mg/L) are the initial and equilibrium Cr (VI) ion concentrations in the aqueous solution, respectively. (L) is the volume of the solution and W (g) is the mass of the adsorbent used.

2.4.3 Batch adsorption experiments for the synthesised de-oiled Moringa oleifera magnetite bionanocomposites.

In order to investigate the adsorption of Cr (VI) on Moringa oleifera seeds functionalised magnetite bionanocomposites ($DMOSFeNP_{H20}$, $DMOSFeNP_{salt}$, and $DMOS_{biocomp}$) the adsorption method was performed under laboratory conditions at standard room temperature and pressure. Adsorption studies were done by preparing different concentration of the Cr (VI) solutions, which was achieved by dilution of the Cr (VI) stock solution at room temperature. Fixed amounts of bionanocomposites (0.02g) were added to 50 ml solutions containing different initial concentration of Cr (VI) ions. The pH of the resultant mixture was adjusted between 4-5 before being transferred to an orbital shaker for 2 hrs at 1200rpm. The resultant mixture was filtered through a Whatman number 42 filter and the supernatant liquid was collected in a 50ml volumetric flask for analysis. The concentration of the Cr (VI) ions was analysed using a Spectrophotometer 300. Before the adsorption experiments, calibration curve for Cr (VI) was run to analyse the Cr (VI) concentration in the analyte. The uptake of the Cr (VI) by the bionanocomposite particles, ($DMOSFeNP_{H20}$, $DMOSFeNP_{salt}$, and $DMOS_{biocomp}$) were calculated using equation (4).

$$q_e \text{ (mg/g)} = \frac{(C_i - C_e)V(mls)}{1000 \times m(g)} \quad (4)$$

where C_i is the initial metal ion concentration (mg/g) and C_e is the equilibrium or final concentration of the Cr (VI) ions at the end of the adsorption period. Data generated was fitted to the adsorption isotherm models to analyse the adsorption properties of the bionanocomposites. Adsorption kinetic studies were done by mixing fixed amount of the bionanocomposites (0.02g) in 20mls of Cr (VI) of different initial concentration of Cr (VI) ions in 50ml conical flasks. Samples were shaken in an orbital shaker for 120mins, pH 5, 120rpm at standard room temperature and pressure. The samples were collected at 30mins intervals and filtered using a Whatman 24 filter before analysed for Cr (VI) ion concentration. Adsorption kinetic rates where fitted to pseudo first and second kinetic models to deduce the reaction mechanisms.

Results and discussion:

3.1 Characterisation of the de-oiled Moringa oleifera bionanocomposites

3.1.1 Point of zero charge

Adsorption of metal ions in solution depends on the solution pH as it affects the metal solubility constants and the surface charge. The solution pH determines the degree of dissociation of the functional groups on the surface of the adsorbent and metal solubility. The point of zero charge is the pH at which the surface of your adsorbent is neutral. Below this value, the surface is positively charged vice versa. The point of zero charge for de-oiled Moringa oleifera is between 4.0 - 6 p H range as shown in Fig. 1. The surface of the bionanocomposite was expected to be positive within this pH range. Adsorption experiments were carried out within this pH range for all the three bionanocomposites.

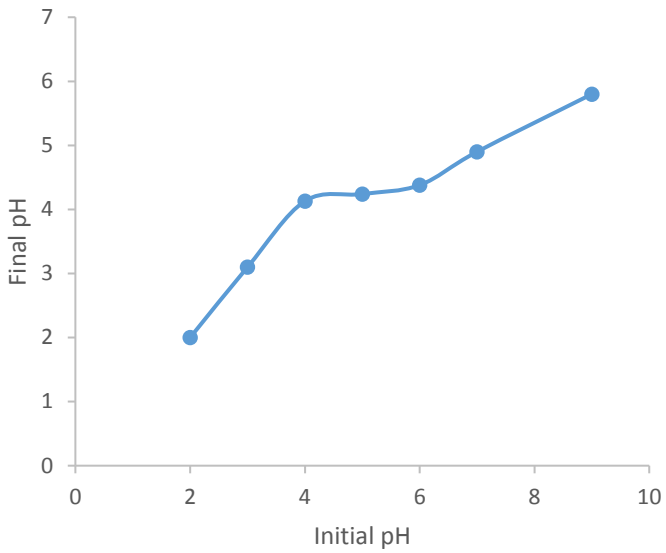

Fig 1.0 Point of zero charge for De-oiled Moringa oleifera seed powder (DMOS)

3.1.2 Pore structure analysis of the bionanocomposites.

The highest average swelling ratio of the de-oiled Moringa oleifera seed was between 300-400µm size on the wet basis and was lowest on dry basis as shown in Fig. 2. The rate of swelling was determined by many physicochemical factors such as porosity and types of porous structure. The most optimum size for the maximum water intake by De-oiled Moringa oleifera seeds occurs between 300-400um. Therefore, for all the experiments, the sieve size range of 300-400um was used for the synthesis of $DMOS_{biocomp}$. The specific surface area of $DMOSFeNP_{H20,}$ $DMOSFeNP_{salt}$, and $DMOS_{biocomp}$ were 50.6, 38.8 and 50.6m^2/g respectively (Table 1.0). The specific surface area for $DMOSFeNP_{H20}$ and $DMOS_{biocomp}$ were found to be similar compared to $DMOSFeNP_{salt}$. This difference could be as a result of coating with organic layer from Moringa oleifera saline extract on the bionanocomposite. Based on the surface area differences, the salt-coated composite was expected to have the least adsorption capacity towards the Cr (VI) ions in solution.

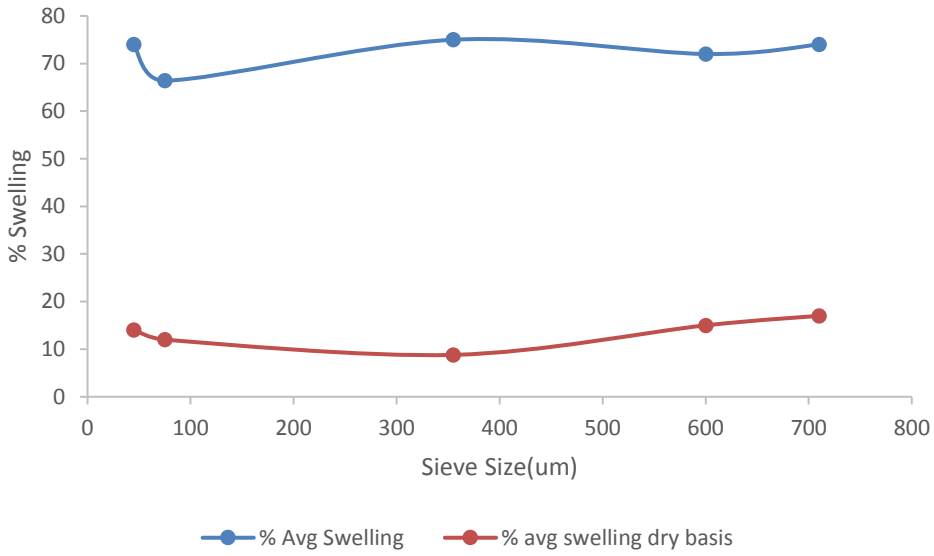

Fig 2.0 Average % swelling of the DMOS in water at different sieve sizes

Table1.0 Surface properties of De-oiled Moringa oleifera seeds bionanocomposites.

Properties	$DMSOFeNP_{salt}$	$DMOSFeNP_{H20}$	$DMOS_{biocomp}$
$S_{BET}(m^2/g)$	$38.7811m^2/g$	$50.6026m^2/g$	$50.5960m^2/g$
Pore volume(V_t)(cm^3/g)	$0.5124cm^3/g$	$1.2598m^3/g$	$0.0837m^3/g$
Pore size	52.85nm	99.59nm	6.619nm

3.1.3 XRD analysis

The crystalline and amorphous phases of the De-oiled Moringa oleifera seeds(DMOS),magnetic $DMOS_{biocomp}$,$DMOSFeNP_{salt}$ and $DMOSFeNP_{H20}$ were characterised by XRD and the results are shown in Fig 3.0. $DMOS_{biocomp}$ revealed characteristic peaks at

around 2θ of 45º which corresponds to magnetite.No peaks observed on the DMOS analysis expect for one peak at 2θ of 25º due to the cellolose(II) crystalline form of the material.The width of this peak may be caused by the presence organic substances such as lignin and hemicellulose see Fig 3.0 below. The average crystalline sizes estimated by Williams Hall method were 17nm,69,21nm and 90,97 for magnetite,DMOSFeNP$_{salt}$ and DMOSFeNP$_{H20}$ respectively.The increase in particles is caused by functionalisation of the magnetite particles with soluble proteins from the two extracts.The XRD patterns described in literature by [38] indicate the presence of intense peaks at 2θ at 30.1º, 35.4º, 42.9º, 57.5º and 67.7º representing the following deffraction patterns of magnetite with cubic spinel crystalline structure.The presence of intense peaks 35.82º and 43.67º representing diffraction patterns 417 and 495 for DMOSFeNPsalt show that magnetite produced is not pure.The same could be observed for DMOSFeNP$_{H20}$ which showed peaks at 30.7º and 35.74º representing diffraction pattern 428 and 187 respectively.Most of the peaks confirm that the bionanocomposites formed is magnetite.

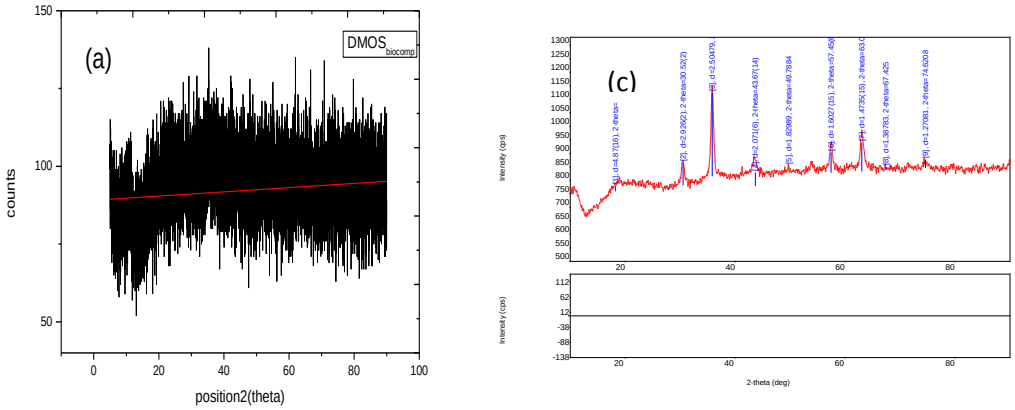

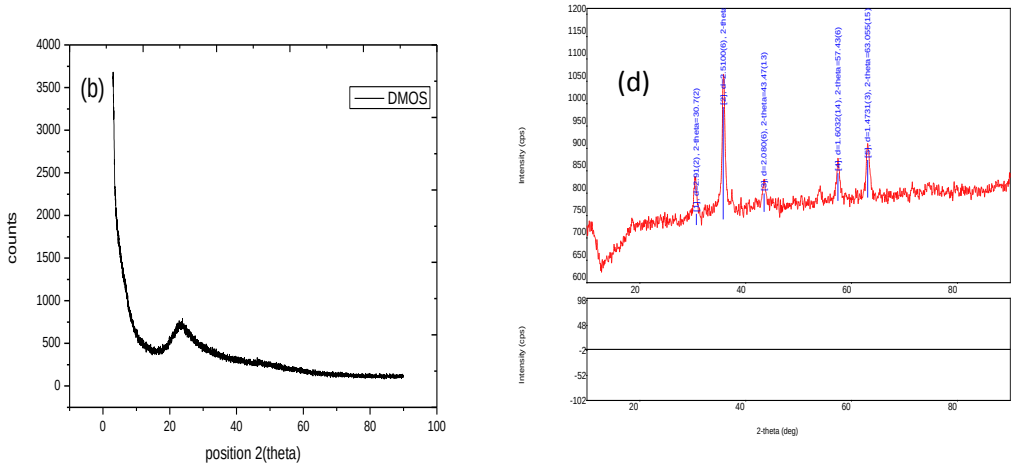

Fig 3.0 XRD pattern of $DMOS_{biocomp}$ (a) DMOS (b), $DMOSFeNP_{salt}$, (c) and $DMOSFeNP_{H20}$, (d)

3.1.4 SEM/EDAX analysis of the bionanocomposites

The morphologies of the biocomposites were characterised by SEM/EDS .Untreated Moringa oleifera seed surfaces are rough, shiny and heterogeneous with rough structures on the surface Fig 4.0 (a),which suggests a potential for Cr(VI) adsorption.This surface appearance suggest the absence of dipole forces which prevents agglomeration and hence a well dispersed surface structure. Surface appearance for the fuctionalised $DMOS_{biocomp}$ was different from the untreated Moringa oleifera seed powder .The $DMOS_{biocomp}$ appeared dark with large clusters due to the stronger magnetic dipole-dipole forces of the Fe_3O_4 particles. The EDS results for the magnetite bionanocomposite show that 90% of the composition is Fe-O see Fig 4.0 (b). The morphologies of $DMOSFeNP_{H20}$ and $DMOSFeNP_{salt}$ were characterised using Scanning Electron Microscope (SEM) Surface images for Moringa oleifera water-soluble and salt soluble crude extracts modified magnetite nano particles are shown in Fig.4.0(c, d).The results show that in (c), the magnetite nanoparticles surface area was reduced by the presence of chloride precipitates on the surface of the magnetite particles.SEM image of the water modified

magnetite nanoparticles in Fig 3,(d) show a large surface area of the magnetite nanoparticles exposed. This phenomenon leads to the conclusion that, surface structure, size distribution and extend of agglomeration are controlled by the type of Moringa seed extracts composition.EDX spectrum for $DMOSFeNP_{H20}$ show that the weight % of Fe and O is higher than $DMOSFeNP_{salt.}$ The results show that in (d) the bionanocomposite particles were highly agglomerated while in (c) were well dispersed respectively. The agglomeration on the former particles can be attributed to stronger magnetic dipole-dipole moments and hence formed large clusters. The presence of sodium chloride on the later disturbed the nuclear growth process, resulting in smaller well-dispersed clusters. The EDS/EDX results in Fig 4.0 indicate that 95% of the material is magnetite

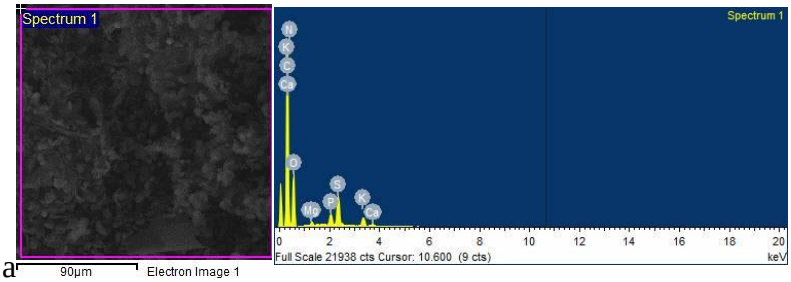

a

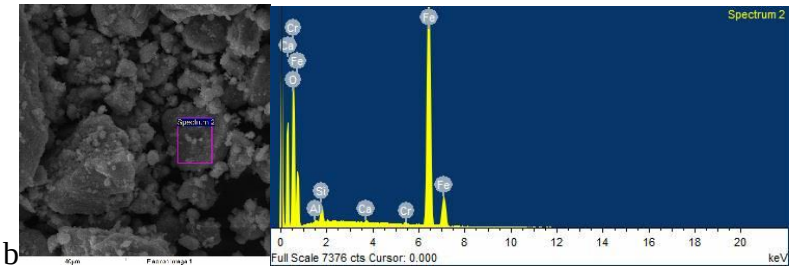

b

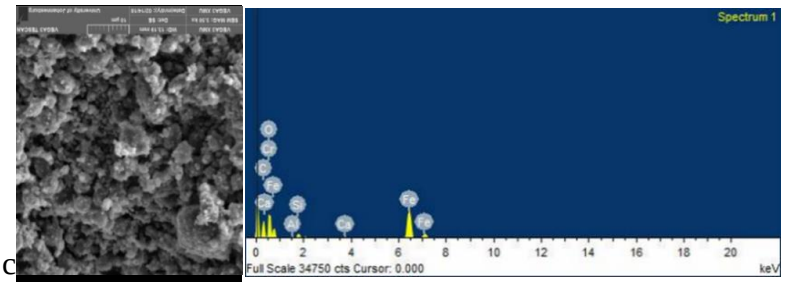

c

d 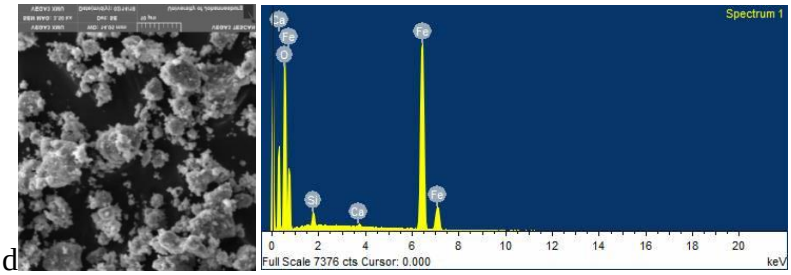

Fig 4.0 SEM/EDX images of the untreated DMOS (a), $DMOS_{biocomp}$ (b), $DMOSFeNP_{salt}$(c), and $DMOSFeNP_{H20}$(d)

3.1.5 FTIR results on unloaded bio nano composites.

Infrared spectra was performed to identify the presence of functional groups on DMOSFeNP $_{salt}$, $DMOSFeNP_{H20}$ and Magnetite. Fig 5.0 shows the various functional groups in the bionanocomposites. For DMOSFeNP $_{salt}$ a band at 1067cm^{-1} is assigned to stretching aromatic groups and the band at 1453cm^{-1} and1531cm^{-1} shows the carboxylic group and amine groups respectively. These bands are due to protein and fatty acids found in the Moringa oleifera seeds [39]. The peaks at 1736cm^{-1} and 1647cm^{-1} indicate the presence of C=O ester and $C=NH_2$ amides groups in the DMOSFeNP $_{salt}$ and $DMOSFeNP_{H20}$ respectively. For DMOS a band at 3271cm^{-1} is assigned to the O-H stretching vibrations. A band at 791cm^{-1} is attributed to N-H bond of the amide groups. For DMOSFeNP $_{salt}$ and DMOSFeNP $_{H20}$ the 1651cm-1 and 1745cm^{-1} are assigned to $C=NH_2$ amide group and C=O ester groups respectively. Normally there is a shift on the functional groups because the functional groups on the bionanocomposites are interacting with magnetite causing less transmittance on the coated magnetite [40].The involvement of the complex protein polymers from the seed extracts in the formation, stabilization and surface functionalisation of the synthesised magnetite nanoparticles can ascertained as we observe a sharp pick shifts at 791cm^{-1}. When the precursor solution ($FeCl_3$) is heated in an inert atmosphere. The magnetite formation starts by rapid precipitation of

$Fe(OH)^{+}$ in water and if the concentration of dissolved oxygen is low in water and pH high slow oxidation takes place, and the dehydroxylation occurs prior to oxidation ,so that the intermediate transfer to crystalline magnetite. The Fe $(OH)^{+}$ is oxidised to form an intermediate complex $[Fe(OH)_3]^{+3}$ which reacts with another $Fe(OH)^{+}$to form $Fe_3O(OH)_4^{2+}$,which has the same ratio of Fe^{2+}/Fe^{3+} of magnetite. The protein compounds in the Moringa seed extracts forms chelating compounds with complex ion species in solution thereby capping the surface of the nanoparticles. There is a general shift in the bands due to samples being in different media. The transmittance weakens between 500-1500cm-^{1} due to the interaction of the seed extracts with the magnetite nanoparticles. More results are explained further by use of the Raman spectra Figure 6.

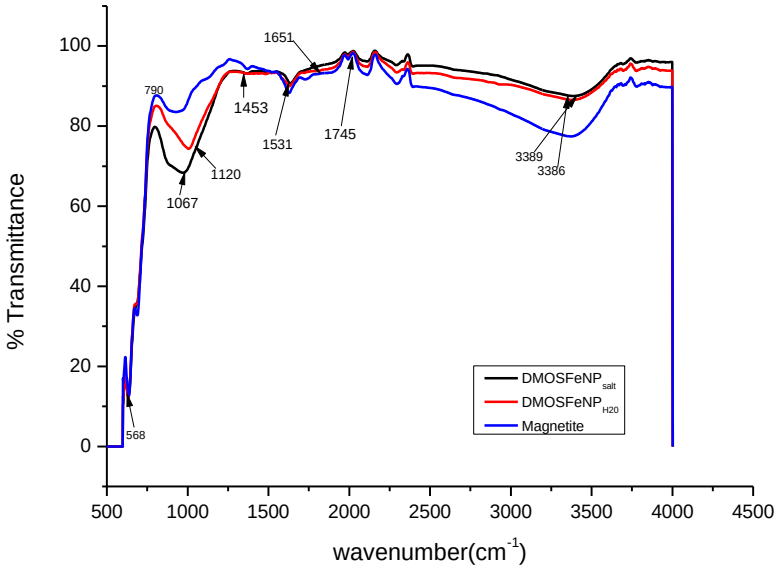

Fig 5.0. FTIR results for $DMOS_{salt}$, $DMOS_{H20}$ and Magnetite

3.1.5.1 FTIR results of Cr (VI) loaded magnetite bionanocomposites.

For the investigation of the removal mechanism of Cr (VI) ions, the FTIR spectra for the un-modified magnetite bionanocomposite particles before and after Cr (VI) loading were compared. The spectra for the modified magnetite bionanocomposite particles are not the same after Cr (VI) adsorption as shown in Fig 5.0 and 6.0 The characteristics peaks at 1398cm^{-1} and 1638cm^{-1} may be assigned to C-O and –R-NH_2 groups of proteins and enzymes in the Moringa seed extract. This shows that the magnetic nanoparticles were modified with oleic acid and the carboxylic acid from the monomer was retained. [41].The infrared band at 1410cm-1 can be assigned to bending vibrations of the O-H bond, which validates the presence of phenolic derivatives such as lignin in the extracts. Amino acid-chromium (VI) interactions can be deduced on the basis of their FTIR results before and after Cr (VI) loading on the magnetite bionanocomposites. Fig 5.0 shows the FTIR spectra of untreated $DMOSFeNP_{salt.}$ showing the presence of O-H stretching vibrations and the contribution for the vibrations of the N-H groups at 3389.15cm^{-1} and 1629.66cm^{-1} due to C=NH_2 amide groups vibrations. The shift of the amine/amide groups in unloaded composite [3389.15cm^{-1}) to [3379.13cm^{-1}] in Cr(VI) treated $DMOSFeNP_{salt}$ confirms ionic interaction between amide groups of the amino acids with the Cr(VI) ions as shown in Fig 6.0.below. A shift on the untreated composite [1629.66cm^{-1}) to [1631.92cm^{-1}) indicate strong ionic interaction of the amine groups with the Cr (VI) ions. The same shift showing strong interaction between Cr(VI) ions with $DMOSFeNP_{H20}$ can observed on the untreated bionanocomposites at [3384.20cm^{-1}) to treated bionanocomposites at [3386cm^{-1}] showing strong interactions of the Cr(VI) with the amine groups. The FTIR spectrum of magnetite nano particles show intense bands at 568cm^{-1}. Therefore, it can be concluded that during the metal ion removal process, there is a chemical reaction-taking place between the adsorbent and adsorbate and it is not physio sorption process**.** Same observations

can be noted for magnetite before loading at [1630.23cm^{-1}] and after loading with Cr (VI) ions at [1635.74cm^{-1}]. Formation of iron nano particles in the DMOSFeNP$_{salt}$ and DMOSFeNP$_{H20}$ can be confirmed by the bands at 567cm^{-1} in Fig 7.0 as shown in Raman spectra.

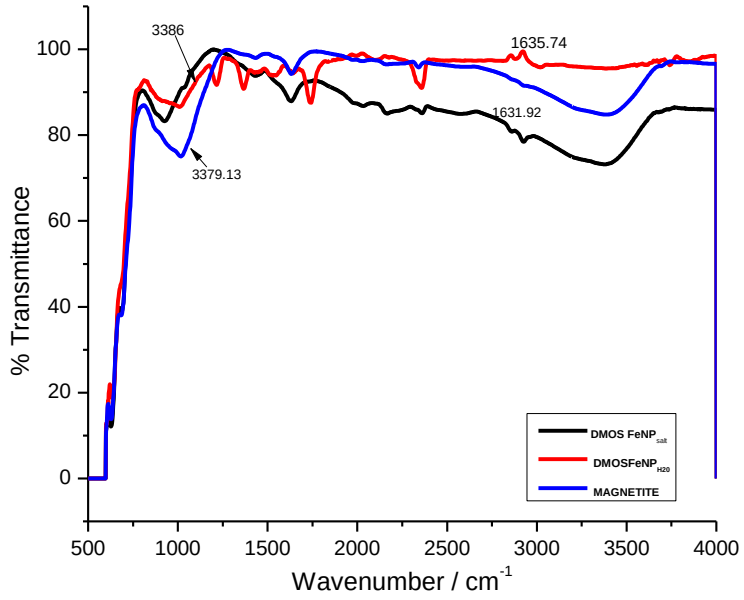

Fig 6. FTIR spectra of Cr (VI) loaded DMSOFeNP$_{salt}$, DMOSFeNP$_{H20}$ and Magnetite

3.1.6 Raman analysis

Raman spectra was performed to identify the nature of chemical bonding and crystallographic orientation of samples on the surface of the DMOSFeNP $_{H20}$ and DMOSFeNP$_{salt.}$ Fig 7.0 shows the two spectra of the bionanocomposites. Series of Raman spectra collected at gradual increase of laser power started for show hematite bands at about 300-400rcm-^{1}. From Fig 7.0 the Raman scattering power of hematite is less than that of magnetite in the DMOSFeNP $_{H20}$ as compared to DMOSFeNP$_{salt}$. As a result, even a very small amount of hematite causes the presence of spurious peaks in the Raman spectrum of magnetite. For DMOSFeNP $_{H20}$ a band at 588,610,630 and 790cm-^{1} confirms the presence of Fe-O vibrations. The same can be observed for the

DMOSFeNP $_{salt}$ on Fig 7.0, (b). Meanwhile, the Raman spectra for DMOSFeNP $_{H20}$ Fig 6.0 also displayed peaks at 3520cm^{-1} for stretching for O-H,at 1616cm^{-1} for the C=C and 1049cm^{-1} for C-O-C adsorption peaks. The presence of O-H in plane bend can be confirmed at band 1356cm^{-1} for the DMOSFeNP$_{H20}$ showing the presence of primary and secondary alcohols in the seed extract. A band at 1410cm-1 for the DMOSFeNPH20 is attributed to bending O-H groups which validates the presence of phenolic derivatives in the water extract. The absence of such peaks on DMOSFeNP$_{salt}$ shows that the water extract is a better media in growing magnetite nanoparticles than salt. Similar results were obtained by Luo et al, 2016 for the degradation of Orange II using grape leaf aqueous extract to synthesis of bimetallic Fe/Pd nanoparticles [42] .

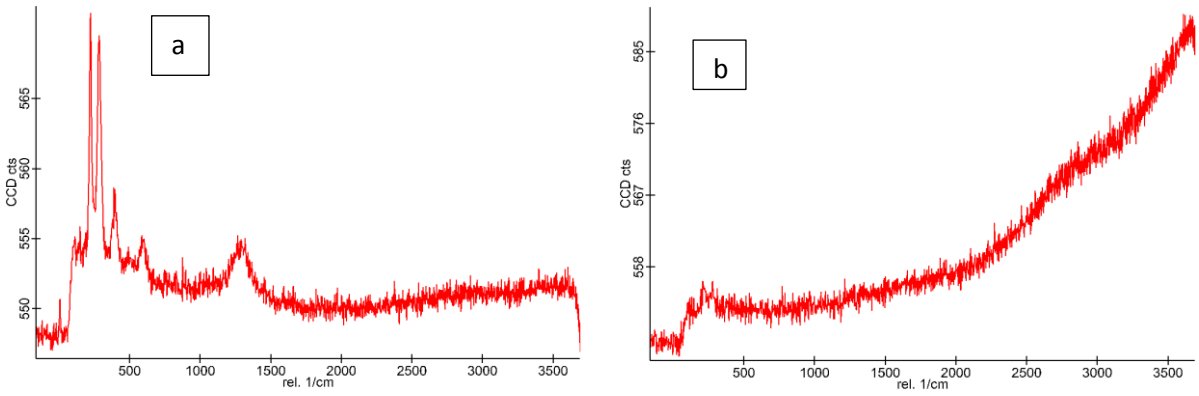

Fig 7.0 Raman spectra DMOSFeNP$_{H20}$ (a), and DMOSFeNP$_{salt}$ (b)

3.1.7 HRTEM analysis

Knowing surface morphology of the nanoparticles is of paramount importance since their surface to volume ratio is a principle feature in nanotechnology. To characterise further the microstructure of the synthesised magnetite nanoparticles, were done using High-resolution TEM analysis (HRTEM). Fig 8.0 below shows perfect lattice fringes in selected regions of

individual particles, which confirms the formation of crystalline magnetite nanoparticle in both samples. The HRTEM image for DMOSFeNP$_{H20}$ are spherical in shape, and well dispersed compared to DMOSFeNP$_{salt}$. Yadav et al. reported similar finding by describing the spherical shape of the iron nano particles prepared from Aloe vara. [43]. This is due to the organic layer from Moringa seed salt extracts covering the surface of the nano particles. EDX spectrum shows the elemental composition of the synthesized bionanocomposites. The % of Fe and O is high in DMOSFeNP$_{salt}$ compared to the DMOSFeNP$_{H20}$.Their stoichiometric ratio does not resemble the pure magnetite nanoparticles and hence the spectrum is consistent with X-ray patterns of the sample showing phase impurity. Presence of extra peaks in the spectrum indicate that this is not recommended method for synthesizing pure magnetite (supplementary notes) The presence of chloride peaks on DMOSFeNP$_{salt}$ confirms the surface morphology, size distribution and extend of agglomeration are controlled by the type of seed extract.

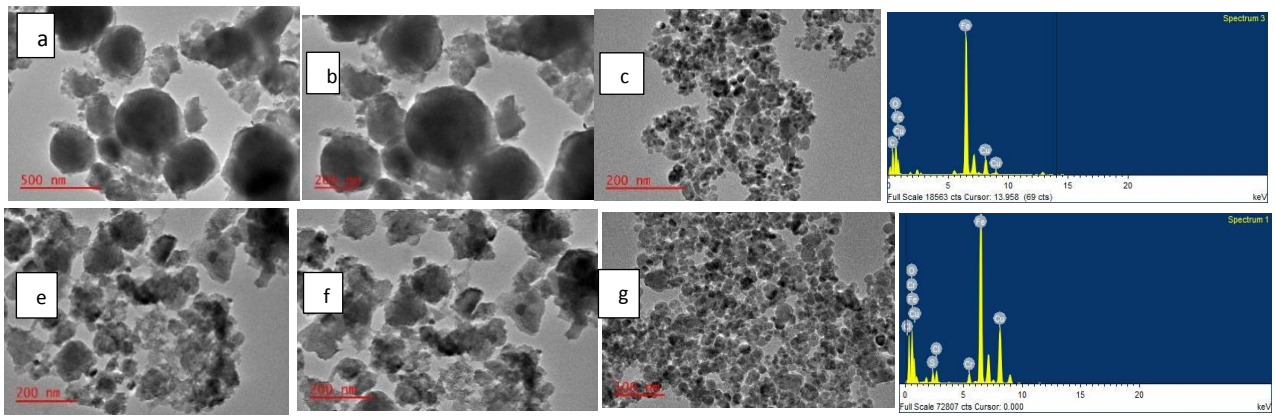

Fig 8.0. HRTEM images of DMOSFeNP$_{H20}$ (a-c), and DMOSFeNP$_{salt}$ (e-g)

3.2 Adsorption studies

3.2.1 Optimisation of the pre-concentration:

The adsorption of the prepared Cr (VI) in aqueous solution was performed using a the three bionanocomposites and the results were compared to untreated Moringa oleifera seeds. In order to obtain the maximum recovery for the determination of Cr (VI), the mass of the composite, pH, extraction time and initial metal ion concentration was investigated, and the results are shown below.

3.2.2 Effect of pH

The pH is the most important parameter to consider in solid-phase extraction process as it affects the surface charges and metal speciation chemistry of the bio-sorbent as shown in Fig.9.0 below. The solution pH affects the degree of dissociation of the carboxyl and hydroxyl functional groups of the adsorbent and the solubility of the Cr (VI) on magnetite bionanocomposites. The effect of pH on Cr (VI) was investigated between 1 to 10 and the results are shown in Fig 9.0 below. The maximum extraction efficiency was obtained at pH range 6-8 which coincide with the point of zero charge for the de-oiled Moringa oleifera seeds. At that p H the surface charge on the Moringa oleifera bionanocomposites is positive which attracts the negatively charged Cr (VI) ions which predominantly exists as CrO^{-}_{4} in abundancy in acidic media.Cr (VI) sorption decreased as the solution pH increased to 8 because as the p H increases the magnetite groups and other functional groups like the carboxylic ,ethers and hydroxyl in the Moringa extracts deprotonate creating a negative surface charge density which reduces the uptake of Cr (VI) from the solution [44].The fluctuation on the $DMOSFeNP_{salt}$ at higher pH can be caused by erosion or degradation of the organic layer at higher pH exposing positive surface which attracts more Cr(VI)

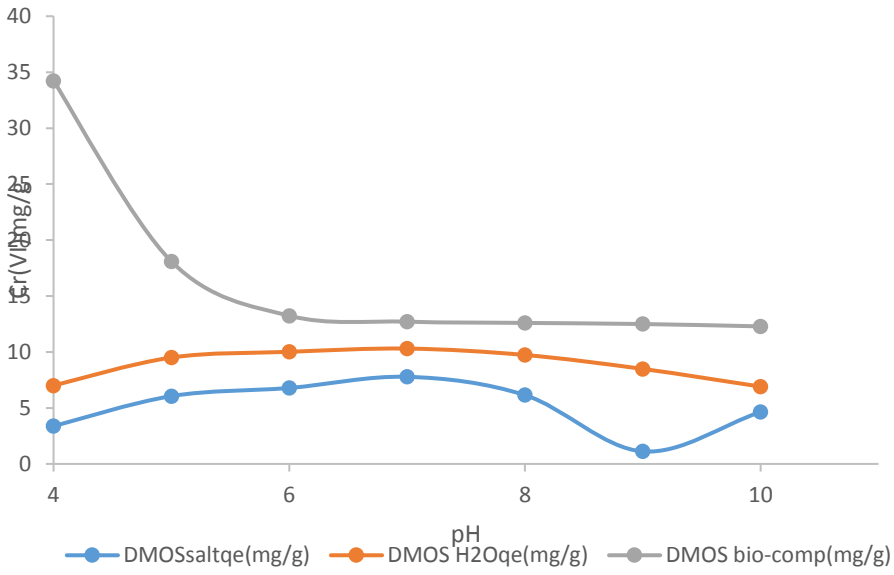

Fig 9.0 Effect of solution pH on Cr (VI) adsorption

3.2.3 Effect of adsorbent dosage

The recoveries of Cr (VI) decreased with increase in dosage quantities for all the three-magnetite bionanocomposites. The adsorption of Cr (VI) was highest at the initial stages of the experiment and decreased gradually as the bio-sorbent dosage increase from 0.01 to 0.07g see Fig 10.0 below This means that the number of ions bound to the adsorbent and the free ions in solution remain constant even if we increase the biosorbent dosages. This indicates poor biomass utilisation efficiency at higher dosages. The results can be explained as a result of partial aggregation, which occurs at high biomass concentrations giving rise to decreased active sites [45].This effect was also reported by [46] for the sago waste for the adsorption of lead and copper .

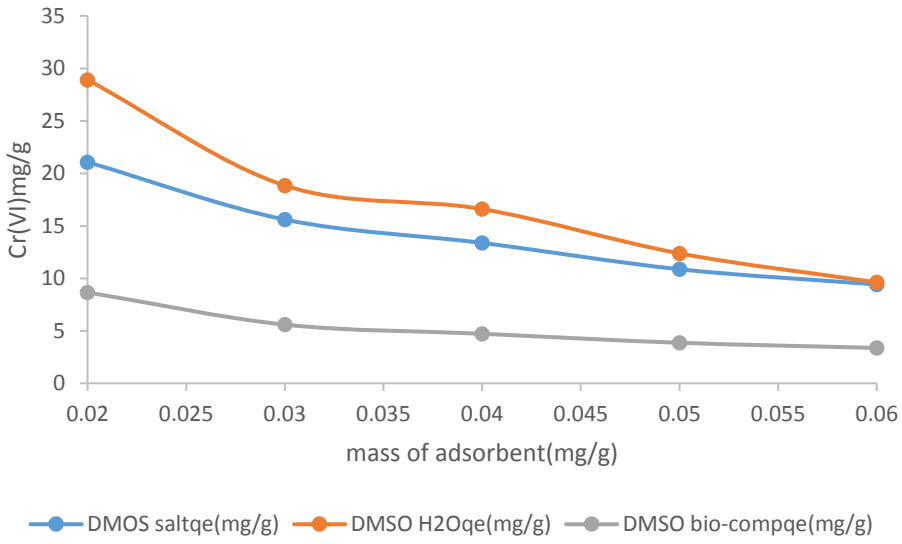

Fig 10.0. Effect of adsorbent dosage on Cr (VI) adsorption

3.2.4 Effect of time

The equilibrium times affect the quantity of pollutant adsorbed over a period of time and the adsorption time was optimised for the recovery of the Cr (VI) ions in solution. The time intervals for the determination of the amount of Cr (VI) adsorbed was kept constant (30mins) for 180 mins as shown in Fig 11.0 below The results show that maximum adsorption took place in the first 60mins contact time with DMOSFeNP$_{H20}$ having the highest adsorption capacity followed by DMOSFeNP$_{salt}$ and lastly DMOS$_{biocomp}$. The high rate of adsorption is due to high surface area and pore volume of DMOSFeNP$_{H20}$ compared to the other two bionanocomposites. It dropped gradually after 1 hour and increases steadily until it reaches equilibrium after 150 mins. This could be due to metal ion adsorption desorption mechanisms over that period or ligand formation followed by rapid Cr (VI) adsorption as time progresses. Therefore, 150 mins is the optimum adsorption time for chromate (VI) ions. Degradation of the organic layer formed on surface of the bionanocomposites can cause fluctuations in Cr (VI)

uptake at higher pH. The DMOSFeNP$_{H20}$ was less affected as compared to DMOS$_{biocomp}$ and DMOSFeNP$_{salt}$.

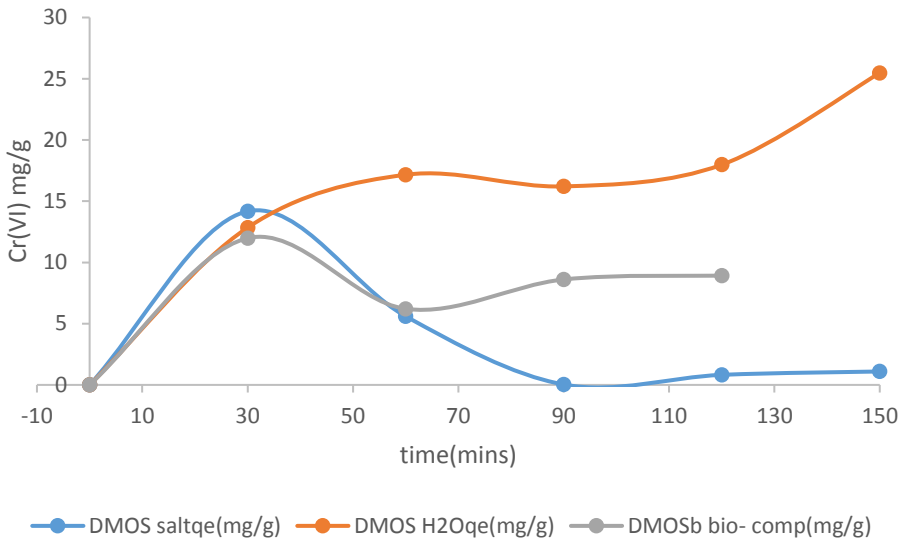

Fig 11.0. Effect of time on Cr (VI) adsorption

3.2.5 Effect of initial concentration of Moringa oleifera bio-composite:

The results of the experiments in Fig 12.0 below show minimum metal removal efficiency with lower initial concentration of the Cr (VI) ions in solution. As the initial concentration of Cr (VI) increases to 20ppm, the amount of Cr (VI) ions adsorbed increases steadily, reaches 10mg/l for the DMOSFeNP$_{H20}$, and is very low for the other two magnetite bionanocomposites. Any further increase in the initial concentration of Cr (VI) from 20ppm resulted in the decrease in the adsorption capacity of Cr (VI) for DMOS$_{biocomp}$ and DMOSFeNP$_{salt}$, while that of DMOSFeNP$_{H20}$ increases. The decrease in adsorption can be attributed to the lower ratio of available sites for Cr (VI) adsorption at higher initial concentration of the Cr (VI) ions. Thus, at low initial concentrations, the removal efficiency is higher and vice versa. When the metal ion concentration increases the reaction sites dwindle but in this case for the Moringa oleifera

magnetite bionanocomposites there seems to be a plentiful supply of these unoccupied sites which allows the adsorption of Cr (VI) to increase with the increase in the initial concentration of the Cr (VI) ions in solution for the DMOSFeNP$_{H20.}$Any drop in adsorption means saturation of the active and an increase in adsorption illustrate availability of active sites for more intake of Cr(VI) ions.

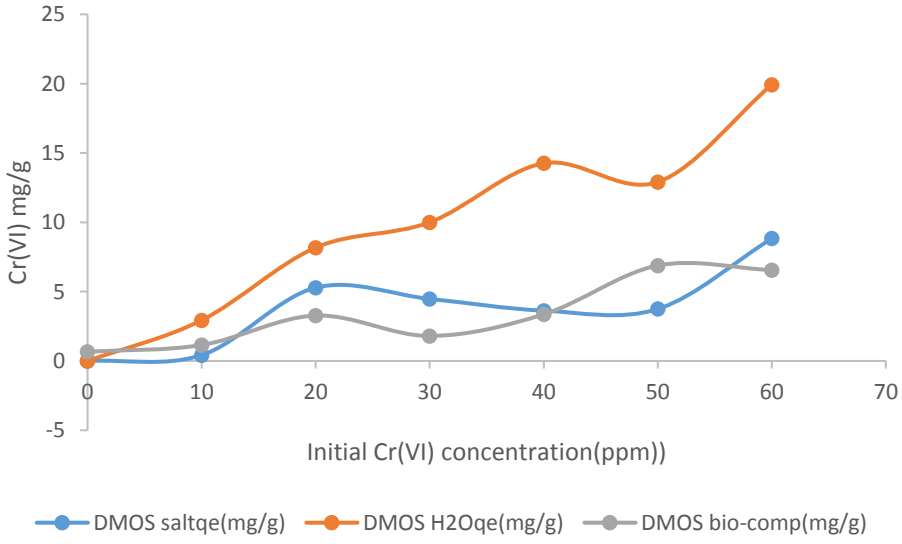

Fig12.0. Effect of initial Cr (VI) concentration Cr (VI) adsorption

3.3 Adsorption isotherm models:

The adsorption of the pollutant onto the surface of the adsorbent is best described using models. In general, an adsorption isotherm is an invaluable curve describing the phenomenon governing the retention (or release) or mobility of a substance from the aqueous porous media or aquatic environments to a solid-phase at a constant temperature and pH [47], [48]. Adsorption equilibrium (the ratio between the adsorbed amount with the remaining in the solution) is

established when an adsorbate containing phase has been contacted with the adsorbent for sufficient time, with its adsorbate concentration in the bulk solution is in a dynamic balance with the interface concentration [49]& [50]. Typically, the mathematical correlation, which constitutes an important role towards the modelling analysis, operational design and applicable practice of the adsorption systems, is usually depicted by graphically expressing the solid-phase against its residual concentration [51].Its physicochemical parameters together with the underlying thermodynamic assumptions provide an insight into the adsorption mechanism, surface properties as well as the degree of affinity of the adsorbents [52].Over the years, a wide variety of equilibrium isotherm models (Langmuir, Fraundlich, Brunauer–Emmett–Teller, Redlich–Peterson, Dubinin–Radushkevich, Temkin, Toth, Koble–Corrigan, Sips, Khan, Hill, Flory–Huggins and Radke–Prausnitz isotherm),have been formulated in terms of three fundamental approaches [53]. Kinetic consideration is the first approach to be referred. Hereby, adsorption equilibrium is defined being a state of dynamic equilibrium, with both adsorption and desorption rates are equal [54]. Whereas, thermodynamics, being a base of the second approach, can provide a framework of deriving numerous forms of adsorption isotherm models [55], [56] and potential theory, as the third approach, usually conveys the main idea in the generation of characteristic curve [57]. However, an interesting trend in the isotherm modelling is the derivation in more than one approach, thus directing to the difference in the physical interpretation of the model parameters [58].The adsorption models chosen for the analysis were Temkin, Langmuir and Freundlich. The Freundlich equilibrium isotherm equation is an empirical equation used for the description of multilayer adsorption with interaction between adsorbed molecules:

$$q_e = k_f C_e^{(1/n)} \qquad (5)$$

where K_f is the Fraundlich isotherm constant $mg^{1-(1/n),}$ $L^{-1/n}g^{-1}$ represents the adsorption intensity, C_e indicates the equilibrium concentration of adsorbate (mg/L), q_e is the amount of adsorbate adsorbed per gram of the adsorbent at equilibrium (mg/g).

The model is applicable to the adsorption on heterogeneous surfaces by a uniform energy distribution and reversible adsorption. The complex nature of the surface of the Moringa oleifera bionanocomposite is shown on Fig 7.0 from (i) to ((j) above. The Fraundlich equation implies that adsorption energy exponentially decreases on the finishing point of adsorptional centres of an adsorbent [59]. The Fraundlich constants are empirical constants depends on many environmental factors. The value of 1/n ranges between 0 and 1 indicates the degree of non-linearity between solution concentration and adsorption [60].If the value of 1/n is equal to 1, the adsorption is linear [61]. Henry's isotherm or one parameter isotherm is applicable for linear adsorption under the condition when n = 1 in Eq. (3). The Langmuir adsorption model was also chosen to estimate the adsorption intensity of the metal ions on the surface of the bio-composite. The Langmuir equation is represented as:

$$\frac{C_e}{Q_e} = \frac{1}{Q_m K_L} + \frac{C_e}{Q_m} \qquad (6)$$

Where C_e is the equilibrium concentration (mgL-1), Q_e is the amount adsorbed at equilibrium (mg/g), Q_m (mg/g) and KL (Lmg/g) are the Langmuir constants related to the adsorption capacity and energy of the adsorption respectively. Fig 13 (a) below shows the linear plot of Ce/Qe vs Ce for the Moringa oleifera composite. The values of Q_m and K_L were determined from the slope and intercept of the linear plot of C_e/Q_e vs. C_e.The experimental data and the correlation coefficients (R^2) values of the composite was -2.10 indicates that the data does not

fit the Langmuir adsorption isotherm refer Table 3.0 below. The Dubini-Radushkevich was also selected to determine the adsorption capacity of the Moringa oleifera composite.Dubinin-Radushkevick isotherm [62], is an empirical model initially conceived for the adsorption of subcritical vapours onto microspore solids following a pore filling mechanism. It is generally applied to express the adsorption mechanism [63], with a Gaussian energy distribution on the heterogeneous surface [64].The model has often successfully fitted high solute activities and the intermediate range of concentrations data well, but has unsatisfactory asymptotic properties and dose not predict the Henry's law at low pressure [65].The approach was usually applied to distinguish the physical and chemical adsorption of metal ions [66],with mean energy,E per molecule of the adsorbate (for removing a molecule from its location in the sorption space to the affinity)can be completed by the relationship [67].

$$E == \left[\frac{1}{\sqrt{2B_{DR}}} \right] \tag{7}$$

where DR is donated as the isotherm constant. Meanwhile, the parameter ε can correlated as:

$$\varepsilon = RTIn\left[1 + \frac{1}{C_e} \right] \tag{8}$$

where R, T and C_e represents the gas constant (8.314J/molK), absolute temperature (K) and adsorbate equilibrium concentration (mg/L), respectively. One of the unique features of the Dubinin-Radushkevich isotherm model lies on the fact that it is temperature –dependent, which when adsorption data at different temperatures are plotted as a function of the logarithm of the amount-adsorbed vs square of the potential energy, all suitable data will lie on the same curve, called the characteristics curve.

3.3.1 Isotherm adsorption models of the de-oiled Moringa oleifera magnetite bionanocomposites.

Linear plots of the isotherm models for the three bionanocomposites are shown Fig 13.0 below. From linear plots for Dubinin-Radushkevich, Fraundlich and Langmuir isotherm models the r, correlation coefficient of fitness was obtained using the lease square plots. For all the plots given the experimental and theoretical values, do not fit the Dubinin-Radushkevich isotherm Model as shown in Fig 13.0. The adsorption model for the $DMOS_{biocomp,}$ $DMOSFeNP_{H2O,}$ $DMOSFeNP_{salt,}$ best fit the Fraundlich, Langmuir and Fraundlich adsorption models respectively as shown in Fig13.0.The r^2 and their corresponding q_{max} values of the magnetite bionanocomposites are given in Table 3.0

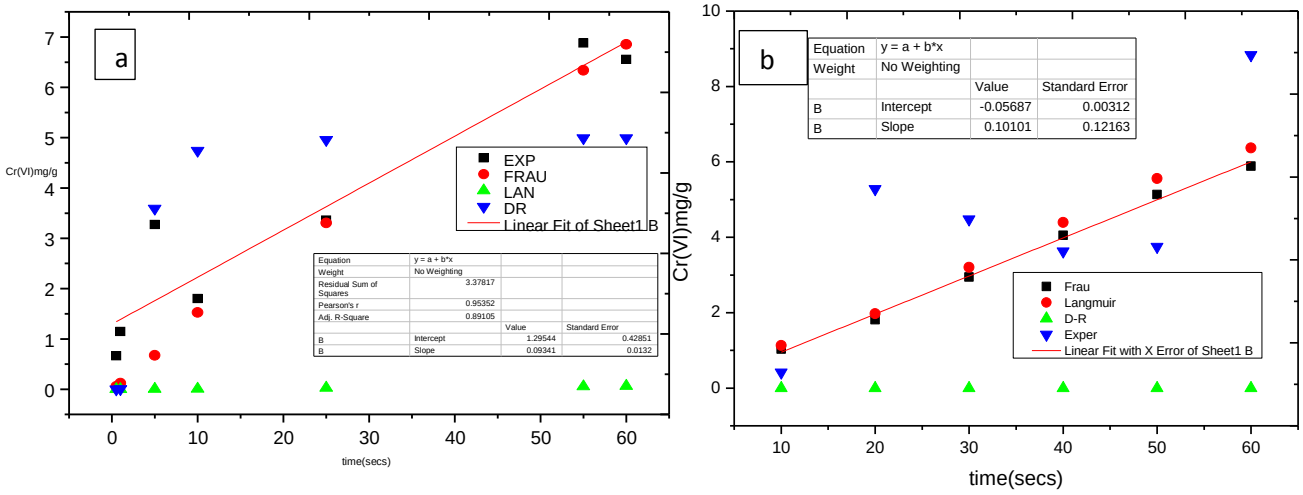

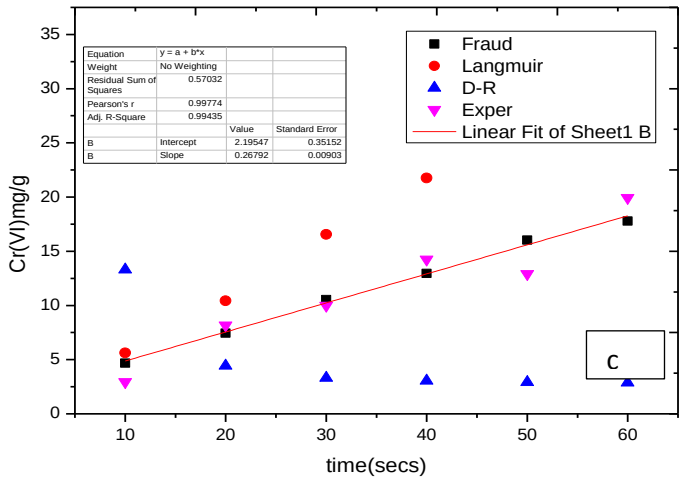

Fig 13. Linear fitting of Langmuir, Fraundlich and Dubinin-Radushkevich isotherm models for $DMOS_{biocomp}$ (a), $DMOSFeN_{Psalt}$, (b) and $DMOSFeNP_{H2O,}$ (c) at different adsorbent initial concentrations.

3.3.2 Summary of the adsorption isotherm models for the composites:

Table 2.0 Parameters of the mathematical models of Langmuir, Freundlich and D-R for the adsorption of Cr (VI) ions on $DMOSFeNP_{H2O,}$ $DMOSFeNP_{salt,}$ DMSO comp and DMOS.

Parameter	**Adsorbent**			
	$DMOSFeNP_{H2O}$	**$DMOSFeNP_{salt}$**	**DMOS $_{biocomp}$**	**DMOS**
Langmuir				
Q_m(mg/g)	33.18	6.37	4.11	3.191
K_L	0.3459	0.1043	0.814	0.089
R^2	0.938	0.67218	-2.102	0.96
K^f	0.75	0.1043	0.25	0.120
n	0.95	1.0069	0.82	0.96
Freundlich				
Q_m(mg/g)	17.79	5.89	6.86	-
R^2	0.999	0.67217	0.770163	0.953

K_d	-0.00002	0.0066	4.876	0.457
q_s	2.7284	-0.0009	5	
D-R				
Q_m(mg/g)	2.87	1.69	2.83	-
R^2	-0.7813	-0.7597	-2.1541	0.968
Q_d	298K	298	298K	$2*e^{-4}$
E	8.314	8.314	8.314	10

Table 3. Comparison of the Cr (VI) adsorption capacity of the four-magnetite bionanocomposites with de-oiled Moringa seeds

Bio sorbent	**q_{max}(mg/g)**	**Adsorption model**	**Kinetic model**	**pH**
De-oiled Moringa seeds	3.19	Langmuir	Second order	5-7
DMOS $_{\text{bio comp}}$	6.86	Fraundlich	Second order	4-5
DMOSFeNP$_{salt}$	6.37	Langmuir	Second order	4-6
DMOSFeNP$_{H2O}$	33.18	Langmuir	First order	4-6

3.3.4 Adsorption kinetic models for Moringa oleifera bio-Composite:

The kinetic study is required to find out the reaction mechanisms and the rate-determining step of the chemical reaction. Experiments were conducted to find out the time required for Cr (VI) adsorption onto the three-bio nanocomposites.

3. 3.5 Pseudo-first order model:

The linear form of the Lagergren pseudo 1st order rate expression is given by the following equation:

$$In(q_e - q_t) = Inq_e - k_1 t \quad (9)$$

Where q_e and q_t are the amount of Cr (VI) adsorbed (mg/g) on the adsorbent at equilibrium and at time t, respectively and K_1 is the rate constant of the first order adsorption (min-1).The plot of In (q_e-q_t) vs. t, gives a straight line as shown in supplementary notes. The rate constant k_1 (min^{-1}) can be calculated from the slope of the linear plots.

3. 3.6 Pseudo-second order model:

The linear form of the pseudo-second order model is described as below:

$$\frac{t}{q^t} = \frac{1}{K_2 q_e^2} + \frac{t}{q_e} \quad (10)$$

where k_2 (g mg^{-1} min^{-1}) is the rate constant of the pseudo-second order kinetic equation, and the q_e and q_t are the amount of Cr (VI) adsorbed (mg/g) onto the Moringa oleifera bio-composite at equilibrium and at time t, respectively. The rate constant k_2 (g mg-1 min -1) and equilibrium adsorption capacity q_e were calculated from the slope and intercept of the linear plot of t (time) vs t/q_t.The results show that $DMOS_{biocomp}$, DMOSFeNPsalt, $DMOSFeNP_{H20}$ and DMOS had r^2 values of 0.99, 0.99, 0.77 and 0.99 which indicate 2nd order,2nd order,1st order and 2nd order kinetic models respectively Fig. 14.0 below.

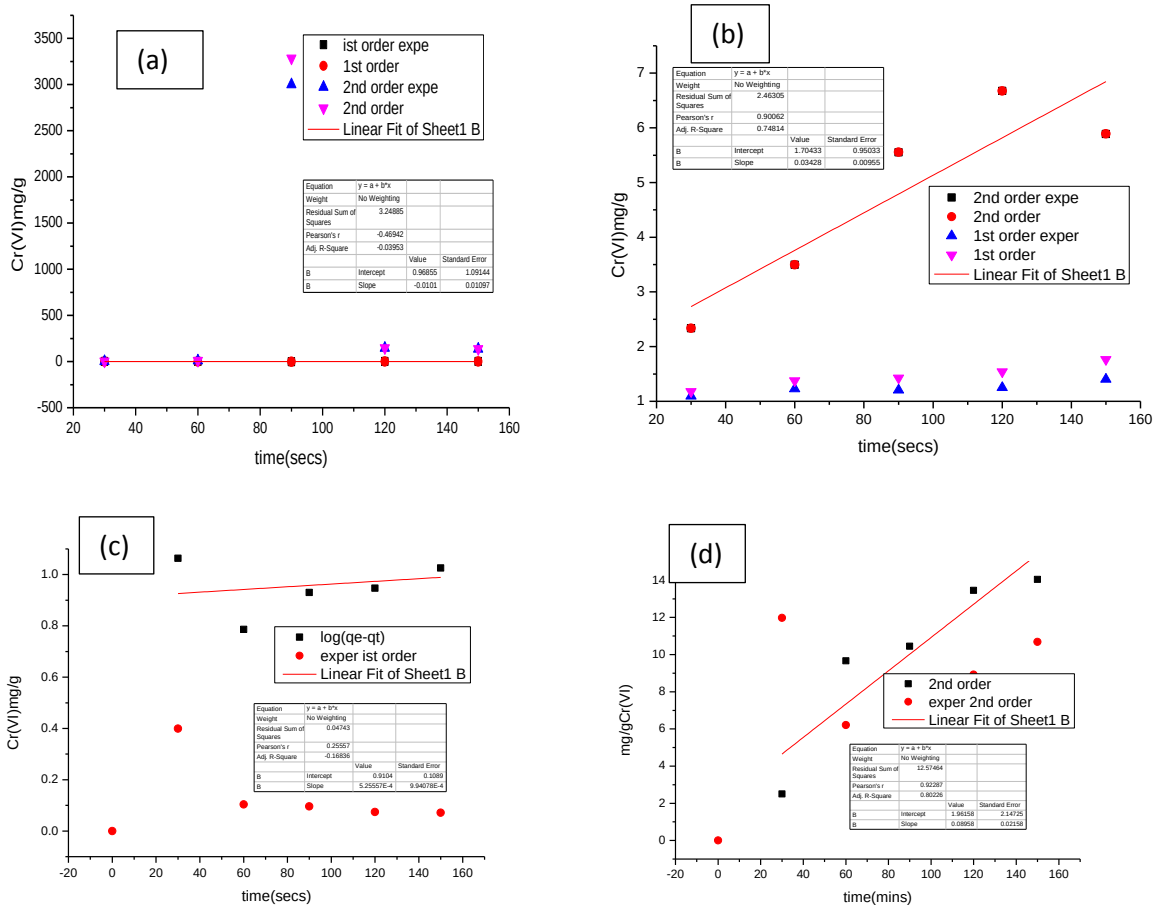

Fig 14.0 Pseudo- first and second-order kinetic models for Cr (VI) adsorption on DMOSFeNPsalt ,(a) and DMOSFeNP$_{H2O}$,(b)and first order for DMOS$_{biocomp}$,(c) and second order DMOS$_{biocomp}$ (d)

Table 1.0 Sorption kinetic parameters of the $DMOSFeNP_{H20}$, $DMOSFeNP_{salt}$ and DMOS for Cr (VI) adsorption

Model	**Parameters**	**DMOS biocomp**	**DMOSFeNP H2O**	**$DMOSFeNP_{salt}$**	**DMOS**
First order	R^2	0.25557	0.770951		-0.944
	k_1	0.0045			-0.0146
	q_e(mg/g)	6.855	33.180	6.370	3.19
Second-order	R^2	0.999921	0.90062	0.9999	0.962
	k_2	0.0989	0.03428	-0.0101	7.22×10^{-3}
	q_e	14.1336			0.781

4.0 Conclusions:

This work represents a simple technique for synthesis of modified Moringa oleifera magnetite nano particles with an average particle size distribution of 15-100nm by a simple precipitation method. BET analysis results showed that the surface area of the synthesised samples are between $25m^2/g$-$50m^2/g$ and the porous distribution determined by BJH method indicate all the prepared samples are mesoporous with pore size range of 2-50nm. It was discovered that the salt extract from the seeds tend to reduce the particle size of magnetite particles by 50% and decrease its surface area by 20% compared to the water extracts. The $DMOSFeNP_{H20}$ showed a good removal efficiency of 33.18mg/g Cr (VI) ions (80%) in solution by its well-dispersed functionalised Moringa oleifera magnetite nano particles as compared to Unfunctionalised

DMOS, $DMOS_{biocomp}$ and $DMOSFeNP_{salt.}$,3.19mg/g, 6.86mg/g and 6.37mg/g respectively. The resulting adsorbent can easily be separated from the pollutant by magnetic separation. The adsorption models for $DMOS_{biocomp}$, $DMOSFeNP_{salt}$ and $DMOSFeNP_{H2O}$ followed Fraundlich, and Langmuir adsorption models respectively. These adsorption isotherm models indicates that the adsorption process occurs in a monolayer and multilayer heterogeneous surface respectively. The kinetic models for $DMOS_{biocomp}$, and $DMOSFeNP_{salt}$ followed second order reaction kinetic however, $DMOSFeNP_{H2O}$ followed first order kinetics The first order kinetics and second order kinetics shows the reaction of Cr (VI) on the magnetite bionanocomposites is physisorption and chemisorption respectively. This shows that adsorption of Cr (VI) takes place via surface exchange reaction mechanisms until all the sites are occupied. Therefore, Moringa seed extracts can be used to support magnetite bionanocomposites for Cr (VI) adsorption. Other potential future research is to synthesis a Moringa oleifera nano magnetic composite, which works on wider pH range.

Acknowledgements

The authors thank The University of Johannesburg South Africa and University of South Africa for financial support on all experimental work. Authors are thankful to Prof.Hennie Grobler for facilitating all experimental work through his Department of Mining Doornfontein Campus University of Johannesburg, South Africa.

References

[1] R.M.Rowel, “Removal of metal ions from contaminated water using agricultural residue.,” *Miscellaneous,* pp. 241-250, 2006.

[2] M. Rehab,A. Hesham, “Potential of using green adsorbent of heavy metal removal from aqueous solutions.,” *Ecological Engineering,* pp. 317-318, 2016.

[3] A. Nisha ,R. Pandey, “Heavy metal and health.,” *Institute of Engineers.,* pp. 1-6, 1984.

[4] D. R.Bartlet, “Behaviour of chromium in soils,” *Environmental Quality Index.,* pp. 31-35, 1979.

[5] P.M.Jardine,M.A. Stewart, M.O. Barnett, “Influence of soil geochemical and physical properties on Cr(VI) sorption and bioaccessibility.,” *Environmental Science and Techology,* vol. 19, no. 47, pp. 11241-11248, 2013.

[6] C.Pan, H. Liu, G. Jeffrey, Z.Wang, “Rates of Cr(VI) generation from CrxFe1-x(OH)3 solids upon reaction with Managanese oxide,” *Environ Science & Technology ,* vol. 21, no. 50, pp. 12416-12423, 2017.

[7] B. Voleski, “Removal of trivalent and hexavalent chromium by seaweed biosorbent.,” *Environmental Science & Technology,* vol. 32, no. 18, pp. 2693-2698, 1998.

[8] A.John, W.James,D.Thomas, “Chromium isotopes and selected trace elements,” Western Mojave Desert,USA, 2008. [Online]. Available: http:?//puds.er.usgs.gov/publication/70033341. [Accessed 2008].

[9] J.Michael,T.Christopher,L.Patrick, “Interaction of chromium(VI) with Aluminium oxide water interface.,” *Physical chemistry C,* vol. 112, no. 6, pp. 2032-2039, 2008.

[10] S.Jiwan,A.S. Kalamdhad, “Effects of heavy metals on soil,plants,human health and aquatic life,a review,” *Res.Chem.Environment.,* vol. 2, no. 1, pp. 15-21, 2011.

[11] M.Sprynskyya, B.Buszewski, A.P. Terzyk, “Study of selection mechanism of heavy metals adsorption on clinoptilolite.,” *Coll.Interf.Scie.,* vol. 304, pp. 21-28, 2006.

[12] T.Adhikari, M.C.Manna,M.V.Singh,R.H.Wanjari, “Bioremeadition measure to minimise heavy metals accumilation in soils and crops irrigated with city efffluent.,” *Food Agricultural Environment,* vol. 2, pp. 266-270, 2004.

[13] S.Y.King,J.U. Moon,S.H. Kim, “Competitive adsorption characteristics of cobalt(II),nickel(II) and Cr(III) by IRN-77 cation exchange resin in synthesised waste water.,” *Chemistry,* vol. 56, pp. 141-147, 2004.

[14] J.Jacobs,R.L.Hardson, J.V. Rouse, “In situ remeadiation of heavy metals using sulfur -based treatment technologies.,” *Hydrovisions,* vol. 10, pp. 1-4, 2001.

[15] E.Vasileva, K. Hadjiivander, “Adsorption of Cr(VI) oxo anions on pure and peroxide modified titanium oxide(anatase),” *Colloid Surface Physiochem Engineering Aspects,* vol. 90, pp. 9-15, 1994.

[16] N.Daneshvar,D.Salari,S.Aber, “Chromium adsorption and Cr(VI) reduction to trivalent chromium in aqueous solution by soya cake.,” *Hazarddous Materials B94,* vol. 94, pp. 49-61, 2002.

[17] Y. N.Shaham, “Photocatalytic reduction of Cr(VI) by titanium oxide coupled to functionalised CNT's.,” *Phys.Chem.,* vol. 44, no. 114, pp. 18946-18952, 2010.

[18] W.Jiang,Q.Cai,W.Xu, “Cr(VI) adsorption and reduction by humic acid coated on magnetite.,” *Enviromental Science Technology,* vol. 48, no. 14, pp. 8078-8085, 2014.

[19] T.Aoki,M.Munemori, “Recovery of Cr(VI) from waste waters with iron (III) hydroxide.,” *Water.Res.,* vol. 16, pp. 793-796, 1982.

[20] J.M Troiano,D.S.Jordan,C.J.Hull,F.M.Gener, “Interaction of Cr(III) and Cr(VI) with haematite studied by second harmonic generation.,” *Physical Chemistry C,* vol. 10, no. 117, pp. 5164-5171, 2013.

[21] X.Guo,G.T.Fei,H.Su,L.D.Zhang, “High performance and reproducible polyaniline nanowire/tubes for the removal of Cr(VI) in aqueous solution.,” *Physical Chemistry C.,* vol. 5, no. 115, pp. 1608-1613, 2011.

[22] J.Valentine,R.B.Garcia,E.Soto Regalado, “Adsorption mechanism of hexavalent chromium from aqueous solutions on modified activated carbon.,” *Environmental Management,* vol. 236, pp. 815-822, 2019.

[23] S.X.Liu,X.Chen,X.Y.Chen,Z.F.Liu, “Acivated carbon with excllent Cr(VI) adsorption performance prepared by acid base surface modifiaction.,” *Hazardous Material,* vol. 1, no. 14, pp. 315-319, 2006.

[24] S.P.Debey,K.Gopal, “Adsorption of Cr(VI) on low cost adsorbents derived from gricultural waste material.,” *Hazardous Material,* vol. 145, pp. 465-470, 2007.

[25] U.R.Malik,S.D.Hasany,M.S.Subhani, “Sorptive potential of sunflower stem for Cr(III) from aqueous solution and its kinetic and thermodynamic profile.,” *Talanta,* vol. 66, pp. 166-173, 2005.

[26] C.L.Batista,E.R.Villanueva,R.V.S.Amorim, “Chromium(VI) ion adsorption features of chitosan film and its zeolites conjugate 13X film.,” *Molecules,* vol. 5, no. 16, pp. 3569-3579, 2011.

[27] M.Ghiaci,R.Kia,A.Abbaspur,F.Seyedeyn-Azad, “Adsorption of chromate by surfactant modified zeolites and MCM-41 molecular sieve.,” *Separtion and purification technology,* vol. 40, pp. 285-295, 2005.

[28] T.S.Shang,J.Zhang,X.J.Jin, “Study of Cr(VI) adsorption onto nitrogen containing activated carbon preparation from bamboo processing residue.,” *Wood Science,* vol. 60, no. 3, pp. 215-224, 2014.

[29] Z.Li,Y.Ge, “Application of lignin and its derivatives in the adsorption of heavy metals ions in water.A review,” *ACS Sustainable Chemistry and Engineering,* vol. 6, no. 5, pp. 1-20, 2018.

[30] C.Han,W.Tang,W.Cai,G.Wang, “Protein assisted hydrothermal synthesis of ultrafine magnetite nanoparticles built porous oriented fibres and their structurally enhanced adsorption to toxic chemical.,” *Material Chemistry,* vol. 21, no. 30, pp. 11188-11196, 2011.

[31] S.Sakar,S.Dutta,P.Bairi,T.Pal, “Redox responsive copper(I) metallogel:a metal-organic hybrid sorbent for the reductive removal chromium(VI) from aqeous solution.,” *Langmuir,* vol. 30, no. 26, p. 78, 2014.

[32] A. Ewecharoen , P. Thiravetyan, E. Wendel, H. Bert, “Nickel adsorption by sodium polyacrylate-grafted activated carbon.,” *Harzadous Material,* no. 171, pp. 335-339, 2015.

[33] P. Wang, H. Zhu, D. Mingiliang, S. Bao, “Structure regulation of silica nanotubes and their adsorption behaviour for heavy metals ions,” *Harzadous Material,* no. 286, pp. 533-544, 2014.

[34] A. Sixen, M. Bhardwaj, T. Allen, “Adsorption of heavy metals from waste water using agricultural waste-industrial waste as adsorbents,” *Water Science,* no. 31, pp. 189-197, 2017.

[35] T.A Kurniawan, G. Chan, W. Lo, “Comparisons of low-cost adsorbents for treating waste water laden with heavy metals,” *Total Environment,* Vols. 2-3, no. 366, pp. 409-426, 2005.

[36] D. Jonhson, K. Haalberg, “Acid mine drainage remeadiation options:A review.,” *Science Total Environment,* vol. 308, pp. 3-14, 2005.

[37] A.V. Luis, H.G. Thiago, A. Gasela, F. Raquel, “Aquatic toxicity of dyes before and after photon-Fenton treatment.,” *Harzardous Materials,* pp. 332-338, 2014.

[38] D. Abass, “Facile sono chemical synthesis of high moment magnetite nanocube,” *Nanoparticles,* pp. 1354-1365, 2013.

[39] M. Pattanayk, P. Navak, *Nano Science Technology ,* vol. 2, pp. 6-9, 2013.

[40] M.M.Kgatitsoe, “Synthesis of magnetic sorbents modified with Moringa Oleifera extracts for removal of organic pollutants,” Wits University, johannesburg, 2018.

[41] K.Liu, J. Nasrallar, L. Chen, L. Huang, “Preparation of CNC-dispersed magnetic nanoparticles and their application in conductive paper,” *Carbohyrates Polymers,* pp. 78-175, 2015.

[42] F.Luo, D. Yang, M. Megharay, “One step green synthesis of bimetallic Fe/Pd nanoparticles used to degrade Orange (II),” *Harzardous Material,* no. 303, pp. 145-153, 2015.

[43] R.S. Yadav, J. Vilcakova, I. Kurikta, “Structural,magnetic,optical,di-electric,electrical and modulus spectroscopic,” *Physics and chemistry,* no. 110, pp. 87-89, 2017.

[44] M.Fazlzadeh , K.Rahmani, A.Zarei, “A novel green synthesi of zerovalent iron nano particles using three plant extracts and their efficient removal of Cr(VI) ions,” *Powder Technology,* vol. 28, pp. 122-130, 2017.

[45] N.M. Saifuddin, K. Palanisamy, “Removal of heavy metals from industrial wastewater using chitosan coated oil palm shell charcoal,” *Biotechnology,* pp. 44-53, 2005.

[46] S.Y. Quek, D.A.G. Wase, C.F. Forster, “The use of Sago waste for the sorption of lead and copper.,” *Water SA,* no. 24, pp. 251-256, 1998.

[47] J. G. V. B. G.Limousin, “Sorption isotherms :a review on physical bases.modelling and measurements,” *Applied Geochem,* pp. 249-275, 2007.

[48] S.J. Allen, G. Mckay, J.P. Porter, “Adsorption isotherm for basic dyes adsorption by peat in single and binary component systems,” *Colloidal Interface Science,* pp. 322-333, 2004.

[49] K. Vasanth Kumar, S.Sivanesan, “Sorption isotherm for sufranin onto rice husk:comparison of linear and non-linear methods,” in *Dyes Pigments*, 2007, pp. 130-133.

[50] M.Ghiaci, A. Abbaspar, R. Kia, “Equilibrium isotherm studies for the adsorption of benzene ,toluene, and phenol onto organo-zeolites,” *Separation and purification technology,* pp. 217-229, 2004.

[51] M. Ncibi, “Applicability of some of the stastiscal tools to predict optimum adsorption isotherm after linear and non-linear regression analysis,” *Hazrd and Material,* pp. 207-212, 2008.

[52] E. Bulut, M. Ozacar, I. Ayhan, “Adsorption of malachite green onto bentonite:equilibrium and kinetic studies and process design,” *Microporous and Mesoporous Materials,* pp. 234-246, 2008.

[53] A.Malek, S. Farool, “Comparison of isotherm models for hydrocarbon adsorption on activated carbon,” *AIChE,* no. 42, pp. 3191-3201, 1996.

[54] I.Langmuir, “The costitution and fundermentals properties of solids and liquids,” *J.Am.Chem.Soc,* pp. 2221-2295, 1916.

[55] J.H.De, “The Dynamical Character of Adsorption,” University of Oxford, London, 1968.

[56] A. L. Myers, J.M. Prausnitz, “Thermodyamics of mixed gas adsorption,” *AlChem,* pp. 121-129, 1965.

[57] M.M. Dubinin, “The potential theory of adsorption of gases and vapors for adsorbents with energetically non-uniform surfaces.,” *Chem.Rev,* pp. 235-266, 1960.

[58] D.M. Ruthven, “Principles of adsorption and adsorption processes,” Newyork, 1984.

[59] H. Fraundlich, “About the adsorption in solution,” *Phys.Chem,* pp. 385-471, 1906.

[60] E.Alpay, “Mass transfer operations,” Ege University, 1987.

[61] G. Mckay, “Use of adsorbents for the removal of pollutants from wasterwaters.,” *CRC Press,* pp. 133-173, 1995.

[62] M.M. Dubinin, L.V. Radushkevich, “The equations of the characteristics curve of the activated charcoal,” *Phys.Chem,* pp. 331-337, 1947.

[63] A. Gunay, E. Arslankanya, “Lead removal from aqueous solution by natural and pretreated clinoptilolite:adsorption equilibrium and kinetics,” *Hazard Material,* pp. 362-371, 2007.

[64] A. Dabrowski, “Adsorption -from theory to practice,” *Advance in colloid and Interphase Sciences,* vol. 93, pp. 135-124, 1993.

[65] A. Alatin, H. Ozbelge, “Use of general purpose adsorption isotherms for heavy metal -clay mineral interaction,” *Colloid and Interface Sciences,* pp. 130-140, 1998.

[66] M.M. Dubanin, “The potential theory of adsorption of gases and vapors for adsorbents with energetically non-unifirm surface,” *Chem.Rev,* pp. 235-266, 1960.

[67] J.P. Hadson, “Physical adsorption isotherms extending from the ultra high vacuum to vapour pressure,” *Phys.Chem,* pp. 2720-2727, 1969.